Pulsed Line Source Response of a Thin Sheet With High-Contrast Dielectric and Conductive Properties—A Time-Domain Analysis

Adrianus T. de Hoop, *Member, IEEE*, Ling Ling Meng, *Student Member, IEEE*, and Li Jun Jiang, *Senior Member, IEEE*

***Abstract*—A methodology is presented for analytically modeling the reflection and transmission of line-source excited pulsed electromagnetic fields at a thin, planar layer with high-contrast dielectric and conductive properties. Closed-form analytic time-domain expressions are derived for the field components in a 2-D setting via an extension of the Cagniard–DeHoop method. The response to the power exponential source and the power exponential monocycle pulse were studied using the newly proposed method.**

***Index Terms*—Cagniard-de Hoop method, high-contrast thin layers, power exponential monocycle pulse, power exponential pulse, pulsed electromagnetic (EM) fields.**

I. Introduction

In THE design of integrated electronic circuits and devices for ultra-high bit-rate signal processing, the research of pulsed electromagnetic (EM)-field signal transmission along thin sheets of highly conducting material is an issue of increasing interest. This holds, in particular, for signals with ultrashort pulse rise times and ultrashort pulse time widths, with spectral content in the terahertz regime. In this regime, the traditional metals can no longer be modeled as perfectly conducting and the associated decay in amplitude and, even more important, the broadening of the pulse shape are issues to be accounted for in the design procedure. The pulse broadening itself is giving rise to limits on the pulse repetition rate in the signals that carry the binary information, because of the resulting pulse crowding.

In this paper, we analyze the pulsed EM-field signal transfer in a canonical model configuration. It consists of a pulsed electric-current line source, oriented parallel to a thin sheet with high contrasts in its conductive and dielectric properties with respect to its embedding free space, that emits an EM field. The electric-field strength of the propagated EM field at some distant point is taken as the received signal. The constitutive properties of the thin sheet are modeled via the thin-sheet, high-contrast boundary conditions that have been derived in [1] (where also references to related methods in the earlier literature can be found). Preliminary results to the problem have been reported in [2]. Closed-form time-domain (TD) expressions for the field components are constructed with the aid of an extension of de Hoop's modification to the Cagniard method for handling pulsed-field propagation in layered media [3]–[7].

Section II contains the description of the configuration and the formulation of the problem. The corresponding problem in the wave slowness domain is constructed in Section III. In Section IV, the solution to the problem in the wave slowness domain is presented. Section V discusses the transformation of this solution back to the space-time domain. Section VI gives two types of line source pulses. Section VII gives a number of illustrative numerical results. Section VIII concludes this paper.

Manuscript received July 21, 2012; revised July 22, 2013; accepted July 30, 2013. Date of publication August 07, 2013; date of current version October 28, 2013. This work was supported in part by the Research Grants Council of Hong Kong (GRF 715011, and 711511), HKU Small Project Funding (201007176196), HKU Seed funding (201102160033), NWO/HKRGC Joint Research Scheme, and in part by the University Grants Council of Hong Kong under Contract AoE/P-04/08).

A. T. de Hoop is with the Faculty of Electrical Engineering, Mathematics and Computer Science Department, Laboratory of Electromagnetic Research, Delft University of Technology, Delft 2628 CD, the Netherlands (e-mail: a.t.dehoop@tudelft.nl).

L. L. Meng and L. J. Jiang are with the Department of Electrical and Electronic Engineering, University of Hong Kong, Hong Kong, China (e-mail: llmeng@eee.hku.hk; jianglj@hku.hk).

Color versions of one or more of the figures in this paper are available online at http://ieeexplore.ieee.org.

Digital Object Identifier 10.1109/TAP.2013.2277577

II. Description of the Configuration and Formulation of the Problem

The position in the configuration is specified by the coordinates $\{x_1, x_2, x_3\} \in \mathbb{R}^3$ with respect to a Cartesian reference frame with the origin $\mathcal{O}$ and the three mutually perpendicular base vectors $\{\boldsymbol{i}_1, \boldsymbol{i}_2, \boldsymbol{i}_3\}$ of unit length each. In the indicated order, the base vectors form a right-handed system. The time coordinate is $t \in \mathbb{R}$. Differentiation with respect to x_m is denoted by ∂_m; ∂_t is a reserved symbol denoting differentiation with respect to t.

A line source of electric current with volume source density

$$J_2(x_1, x_3, t) = I(t)\delta(x_1, x_3 - h) \tag{1}$$

electric current $I(t)$ and located at $\{x_1 = 0, -\infty < x_2 < \infty, x_3 = h\}$, with $h > 0$, in a homogeneous, isotropic, lossless medium with electric permittivity $\epsilon > 0$ and magnetic permeability $\mu > 0$, generates a 2-D, x_2-independent, EM field with nonvanishing components $\{H_1, E_2, H_3\}(x_1, x_3, t)$. The pertaining EM-field equations are

$$\partial_1 H_3 - \partial_3 H_1 + \epsilon\,\partial_t E_2 = -I(t)\delta(x_1, x_3 - h), \tag{2}$$

$$\partial_1 E_2 + \mu\,\partial_t H_3 = 0, \tag{3}$$

$$\partial_3 E_2 - \mu\,\partial_t H_1 = 0. \tag{4}$$

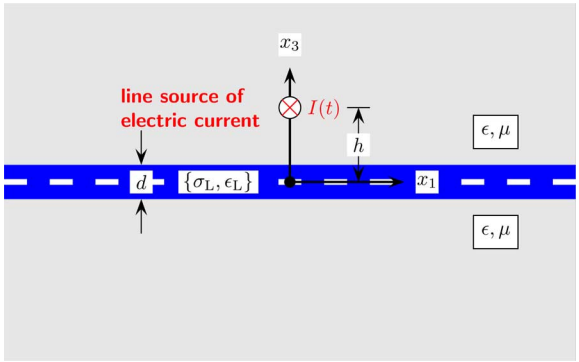

Fig. 1. Configuration with the highly contrasting thin sheet.

In the plane $\{x_3 = 0\}$, a thin layer of vanishingly small thickness d and with high contrasts in dielectric and conductive properties is present as shown in Fig. 1. Its properties are modeled via the thin-sheet boundary conditions [1]

$$\begin{aligned}&\lim_{x_3\downarrow 0} E_2(x_1, x_3, t)\\ &\quad = \lim_{x_3\uparrow 0} E_2(x_1, x_3, t)\\ &\quad = E_2(x_1, 0, t) \text{ for all } x_1 \in \mathbb{R}, t \in \mathbb{R}, \end{aligned} \tag{5}$$

$$\begin{aligned}&\lim_{x_3\downarrow 0} H_1(x_1, x_3, t) - \lim_{x_3\uparrow 0} H_1(x_1, x_3, t)\\ &\quad = (G_{\rm L} + C_{\rm L}\partial_t) E_2(x_1, 0, t) \text{ for all } x_1 \in \mathbb{R}, t \in \mathbb{R}\end{aligned} \tag{6}$$

where

$$G_{\rm L} = \lim_{d\downarrow 0} \int_{x_3=-d/2}^{d/2} \sigma_{\rm L}(x_3) {\rm d}x_3 \tag{7}$$

where $\sigma_{\rm L}(x_3)$ is the electric conductivity of the layer and

$$C_{\rm L} = \lim_{d\downarrow 0} \int_{x_3=-d/2}^{d/2} \epsilon_{\rm L}(x_3) {\rm d}x_3 \tag{8}$$

where $\epsilon_{\rm L}(x_3)$ is the electric permittivity of the layer.

It is assumed that the electric current excitation starts to act at the instant $t = 0$ and that prior to this instant, the field quantities vanish throughout the configuration (initial condition).

III. Field Problem in the Wave Slowness Domain

The problem is solved with the aid of an extension of de Hoop's modification [5] of the Cagniard technique [3], [4]. It yields closed-form time-domain expressions for the field components in the configuration. Exploiting the time invariance of the configuration and the causality of the source and field quantities, the method starts with the one-sided *time Laplace transformation*

$$\begin{aligned}&\{\hat{H}_1, \hat{E}_2, \hat{H}_3\}(x_1, x_3, s)\\ &\quad = \int_{t=0}^{\infty} \exp(-st) \{H_1, E_2, H_3\}(x_1, x_3, t) {\rm d}t\\ &\qquad\qquad \text{for } s \in \mathbb{C},\ {\rm Re}(s) > 0.\end{aligned} \tag{9}$$

The transforms in the left-hand side are *analytic* in the right-half $\{s \in \mathbb{C}, {\rm Re}(s) > 0\}$ of the complex s-plane (Fig. 2). In view

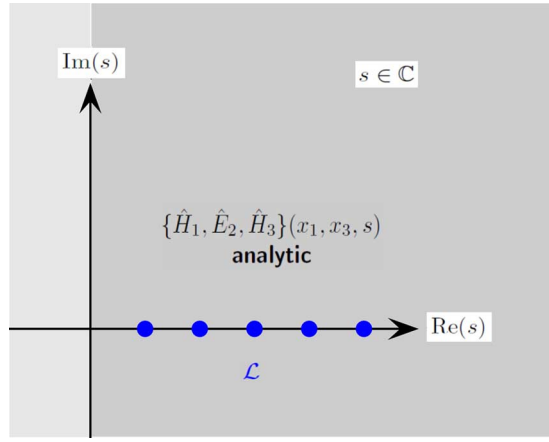

Fig. 2. Domain of analyticity and Lerch sequence in the complex time Laplace transform plane.

of *Lerch's theorem* ([8, 63–65], the interrelation between the time-domain functions and their Laplace transform's counterparts is unique when the latter are specified at the sequence of equidistant values of the transform parameter s (Fig. 2)

$$\mathcal{L} = \{s \in \mathbb{R}; s = s_0 + n\,h, s_0 > 0, h > 0, n = 0, 1, 2, \ldots\} \quad \text{(Lerch sequence)} \tag{10}$$

on the positive real s-axis. (Note that in this theorem, *causality* is a decisive property.) Under the transformation (9) and the zero-value initial conditions, the operator ∂_t is replaced with a multiplication by s. Furthermore

$$\{\hat{H}_1, \hat{E}_2, \hat{H}_3\}(x_1, x_3, s)|_{s\in\mathcal{L}} \in \mathbb{R} \tag{11}$$

a property that is needed in our later analysis. Next, the spatial shift invariance of the configuration in the x_1-direction enables the use of the *wave slowness representation*

$$\begin{aligned}&\{\hat{H}_1, \hat{E}_2, \hat{H}_3\}(x_1, x_3, s)\\ &\quad = \frac{s}{2\pi {\rm i}} \int_{p=-{\rm i}\infty}^{{\rm i}\infty} \exp(-spx_1) \{\tilde{H}_1, \tilde{E}_2, \tilde{H}_3\}(p, x_3, s) {\rm d}p\end{aligned} \tag{12}$$

where p is the (complex-valued) wave slowness parameter. Through this representation, the operator ∂_1 is replaced with $-sp$. Furthermore, using the properties of the Dirac delta distribution

$$\tilde{J}_2(p, x_3, s) = \hat{I}(s)\delta(x_3 - h). \tag{13}$$

With this, the field (2)–(4) transform into

$$-sp\tilde{H}_3 - \partial_3\tilde{H}_1 + s\,\epsilon\,\tilde{E}_2 = -\hat{I}(s)\delta(x_3 - h) \tag{14}$$

$$-sp\tilde{E}_2 + s\,\mu\,\tilde{H}_3 = 0 \tag{15}$$

$$\partial_3\tilde{E}_2 - s\mu\,\tilde{H}_1 = 0 \tag{16}$$

and the boundary conditions (5)–(6) into

$$\begin{aligned}&\lim_{x_3\downarrow 0} \tilde{E}_2(p, x_3, s) = \lim_{x_3\uparrow 0} \tilde{E}_2(p, x_3, s)\\ &\quad = \tilde{E}_2(p, 0, s)\end{aligned} \tag{17}$$

$$\begin{aligned}&\lim_{x_3\downarrow 0} \tilde{H}_1(p, x_3, s) - \lim_{x_3\uparrow 0} \tilde{H}_1(p, x_3, s)\\ &\quad = (G_{\rm L} + s\,C_{\rm L})\tilde{E}_2(p, 0, s).\end{aligned} \tag{18}$$

IV. Wave Slowness-Domain Field Expressions

Defining the *incident field* $\{H_1^{\rm i}, E_2^{\rm i}, H_3^{\rm i}\}$ as the field that would exist in the absence of the contrasting layer, (14)–(16) lead to

$$\partial_3^2 \tilde{E}_2^{\rm i} - s^2\gamma^2(p)\tilde{E}_2^{\rm i} = s\,\mu\,\hat{I}(s)\delta(x_3 - h) \tag{19}$$

where

$$\gamma = (c^{-2} - p^2)^{1/2} \tag{20}$$

with $\gamma > 0$ for $p \in \mathbb{I}$ and

$$c = (\epsilon\,\mu)^{-1/2}. \tag{21}$$

From (19), it follows that:

$$\tilde{E}_2^{\rm i} = \mu\,\hat{I}(s)\,\frac{\exp\left[-s\gamma(p)X_3^{\rm i}\right]}{2\,\gamma(p)} \tag{22}$$

where $X_3^{\rm i} = |x_3 - h|$. In the half-space $\{(x_1, x_2) \in \mathbb{R}^2, x_3 > 0\}$, we now write the total field as the sum of the incident and the *reflected field* $\{H_1^{\rm r}, E_2^{\rm r}, H_3^{\rm r}\}$. In the half-space $\{(x_1, x_2) \in \mathbb{R}^2, x_3 < 0\}$, we denote the total field as the *transmitted field* $\{H_1^{\rm t}, E_2^{\rm t}, H_3^{\rm t}\}$. Taking into account that the reflected field and the transmitted field travel away from the scattering thin layer, we write their electric-field wave slowness representation as

$$\tilde{E}_2^{\rm r} = \mu\,\tilde{R}(p,s)\hat{I}(s)\,\frac{\exp\left[-s\gamma(p)X_3^{\rm r}\right]}{2\,\gamma(p)} \tag{23}$$

where $X_3^{\rm r} = x_3 + h$, with $x_3 > 0$, and

$$\tilde{E}_2^{\rm t} = \mu\,\tilde{T}(p,s)\hat{I}(s)\,\frac{\exp\left[-s\gamma(p)X_3^{\rm t}\right]}{2\,\gamma(p)} \tag{24}$$

where $X_3^{\rm t} = h - x_3$, with $x_3 < 0$. In (23), $\tilde{R}(p,s)$ is the *wave slowness domain reflection coefficient*; in (24), and $\tilde{T}(p,s)$ is the *wave slowness domain transmission coefficient*. Using (22)–(24) in (15)–(16) and substituting the result in the boundary conditions (17)–(18), we obtain

$$\tilde{R}(p,s) = -1 + \tilde{T}(p,s), \tag{25}$$

$$\tilde{T}(p,s) = \frac{\beta_{\rm L}(p)}{\beta_{\rm L}(p) + G_{\rm L}/C_{\rm L} + s} \tag{26}$$

with

$$\beta_{\rm L}(p) = \frac{2\,\gamma(p)}{\mu\,C_{\rm L}}. \tag{27}$$

V. Space-Time Expressions for the Electric-Field Constituents

Based on (22)–(24), the expressions for the time Laplace transformed electric-field constituents are written as

$$\hat{E}_2^{\rm i,r,t}(x_1, x_3, s) = s\,\mu\,\hat{I}(s)\hat{G}^{\rm i,r,s}(x_1, x_3, s) \tag{28}$$

where

$$\hat{G}^{\rm i}(x_1, x_3, s) = \frac{1}{2\pi{\rm i}}\int_{p=-{\rm i}\infty}^{{\rm i}\infty} \frac{\exp\left\{-s\left[px_1 + \gamma(p)X_3^{\rm i}\right]\right\}}{2\,\gamma(p)}{\rm d}p, \tag{29}$$

$$\hat{G}^{\rm r}(x_1, x_3, s) = \frac{1}{2\pi{\rm i}}\int_{p=-{\rm i}\infty}^{{\rm i}\infty} \tilde{R}(p,s)\frac{\exp\left\{-s\left[px_1 + \gamma(p)X_3^{\rm r}\right]\right\}}{2\,\gamma(p)}{\rm d}p, \tag{30}$$

$$\hat{G}^{\rm t}(x_1, x_3, s) = \frac{1}{2\pi{\rm i}}\int_{p=-{\rm i}\infty}^{{\rm i}\infty} \tilde{T}(p,s)\frac{\exp\left\{-s\left[px_1 + \gamma(p)X_3^{\rm t}\right]\right\}}{2\,\gamma(p)}{\rm d}p \tag{31}$$

are the corresponding Green's function constituents. Note that the integrands, considered as a function of p and with s real and positive, have no poles in the complex p-plane, only the branch points at $p = \mp c^{-1}$. This is indicative for the absence of true surface waves like, for example, in elastodynamics, the Rayleigh wave at the stress-free boundary of an elastic solid, the Scholte wave at a fluid/solid boundary, and the Stoneley wave at the interface of two elastic solids. This does, however, not imply that no large surface effects can occur.

The time-domain counterparts of (29)–(31) are determined with the aid of an extension of the standard Cagniard-de Hoop method [5]. Accordingly, the integrands in the integration with respect to p are, away from the imaginary axis, continued analytically into the complex p-plane, cut along the branch cuts $\{1/c < |{\rm Re}(p)| < \infty, {\rm Im}(p) = 0\}$, taking ${\rm Re}([\gamma(p)] > 0$ for all p in the cut plane. Under the application of Cauchy's theorem and Jordan's lemma ([9, p. 1054–1056] of complex function theory, the integration along the imaginary p-axis is replaced with one along the hyperbolic path ("modified Cagniard" or "Cagniard-DeHoop" path, as shown in Fig. 3)

$$px_1 + \gamma(p)X_3 = \tau \text{ for } T < \tau < \infty \tag{32}$$

where $X_3 > 0, T = D/c$ and $D = (x_1^2 + X_3^2)^{1/2} > 0$, while τ replaces p as the variable of integration. In the relevant Jacobian, the relation

$$\partial p/\partial\tau = {\rm i}\gamma(p)/(\tau^2 - T^2)^{1/2} \tag{33}$$

is used.

Next, Schwarz's reflection principle of complex function theory is used to combine the integrations in the upper and lower halves of the complex p-plane. Parametrizing the upper part of the modified Cagniard path through

$$\overline{p}(x_1, X_3, \tau) = \frac{x_1}{D^2}\tau + {\rm i}\frac{X_3}{D^2}(\tau^2 - T^2)^{1/2} \quad \text{for } T < \tau < \infty \tag{34}$$

which has the consequence that

$$\overline{\gamma}(x_1, X_3, \tau) = \gamma[\overline{p}(x_1, X_3, \tau)] = \frac{X_3}{D^2}\tau - {\rm i}\frac{x_1}{D^2}(\tau^2 - T^2)^{1/2} \quad \text{for } T < \tau < \infty \tag{35}$$

and (29) leads to

$$\hat{G}^{\rm i}\left(x_1, X_3^{\rm i}, s\right) = \frac{1}{2\pi}\int_{\tau=T^{\rm i}}^{\infty} \exp(-s\tau)\frac{1}{(\tau^2 - T^{\rm i2})^{1/2}}{\rm d}\tau \tag{36}$$

and (30) to

$$\hat{G}^{\rm r}\left(x_1, X_3^{\rm r}, s\right) = \frac{1}{2\pi}\int_{\tau=T^{\rm r}}^{\infty} \exp(-s\tau) \times {\rm Re}\left[-1 + \frac{\beta_{\rm L}(\overline{p}^{\rm r})}{\beta_{\rm L}(\overline{p}^{\rm r}) + G_{\rm L}/C_{\rm L} + s}\right]\frac{1}{(\tau^2 - T^{\rm r2})^{1/2}}{\rm d}\tau \tag{37}$$

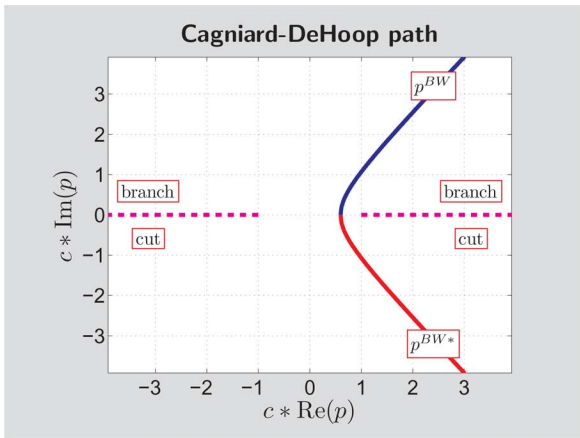

Fig. 3. Cagniard-DeHoop path of integration in the complex slowness plane $(x_1/X_3 = 0.75)$.

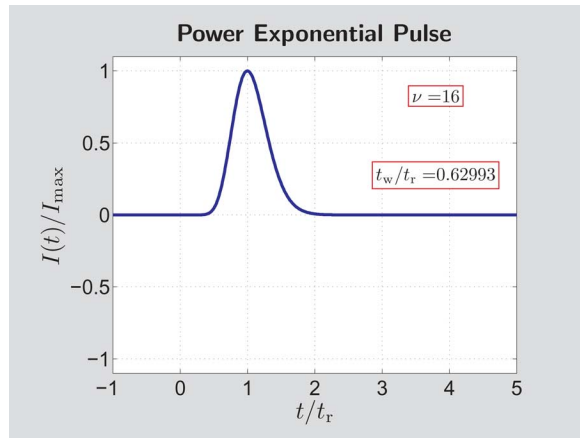

Fig. 4. Example of a power exponential pulse.

and (31) to

$$\hat{G}^{\mathrm{t}}\left(x_1, X_3^{\mathrm{t}}, s\right) = \frac{1}{2\pi}\int_{\tau=T^{\mathrm{t}}}^{\infty} \exp(-s\tau) \times \mathrm{Re}\left[\frac{\beta_{\mathrm{L}}(\overline{p}^{\mathrm{t}})}{\beta_{\mathrm{L}}(\overline{p}^{\mathrm{t}}) + G_{\mathrm{L}}/C_{\mathrm{L}} + s}\right] \frac{1}{(\tau^2 - T^{\mathrm{t}2})^{1/2}} \mathrm{d}\tau \quad (38)$$

where (25)–(27) have been used and the superscripts $^{\mathrm{i,r,t}}$ refer to the incident, reflected, and transmitted wave constituents, respectively.

In (34), Lerch's uniqueness theorem of the one-sided Laplace transformation ([8, pp. 63–65] directly yields

$$G^{\mathrm{i}}\left(x_1, X_3^{\mathrm{i}}, t\right) = \frac{1}{2\pi(t^2 - T^{\mathrm{i}2})^{1/2}} H(t - T^{\mathrm{i}}). \quad (39)$$

If in (37) and (38), the term in brackets in the integrands had been independent of s, Lerch's theorem would, here as well, directly provide the corresponding functions of time. With the aid of the Schouten–Van der Pol theorem of the one-sided Laplace transformation [10], [11, pp. 124–126], [12], and [13, pp. 232–236], we proceed further, however, and apply further rules of the inverse Laplace transformation to obtain

$$G^{\mathrm{r}}\left(x_1, X_3^{\mathrm{r}}, t\right) = \left[-\frac{1}{2\pi(t^2 - T^{\mathrm{r}2})^{1/2}} + \frac{1}{2\pi}\int_{\tau=T^{\mathrm{r}}}^{t} \mathrm{Re}\{\beta_{\mathrm{L}}(\overline{p}^{\mathrm{r}}) \times \exp\{-[\beta_{\mathrm{L}}(\overline{p}^{\mathrm{r}}) + G_{\mathrm{L}}/C_{\mathrm{L}}](t-\tau)\}\} \times \frac{1}{(\tau^2 - T^{\mathrm{r}2})^{1/2}} \mathrm{d}\tau\right] H(t - T^{\mathrm{r}}) \quad (40)$$

and

$$G^{\mathrm{t}}\left(x_1, X_3^{\mathrm{t}}, t\right) = \left[\frac{1}{2\pi}\int_{\tau=T^{\mathrm{t}}}^{t} \mathrm{Re}\{\beta_{\mathrm{L}}(\overline{p}^{\mathrm{t}}) \times \exp\{-[\beta_{\mathrm{L}}(\overline{p}^{\mathrm{t}}) + G_{\mathrm{L}}/C_{\mathrm{L}}](t-\tau)\}\} \times \frac{1}{(\tau^2 - T^{\mathrm{t}2})^{1/2}} \mathrm{d}\tau\right] H(t - T^{\mathrm{t}}). \quad (41)$$

(Note that due to the presence of τ in $\beta_{\mathrm{L}}(\overline{p}^{\mathrm{r,t}})$, the right-hand sides of (40) and (41) are not time convolutions.) Since $\beta_{\mathrm{L}}(\overline{p}^{\mathrm{r,t}})$ is complex-valued, its occurrence in the exponential function is expected to lead to oscillatory phenomena whose magnitude is the more pronounced the larger the imaginary part of $\beta_{\mathrm{L}}(\overline{p}^{\mathrm{r,t}})$ is with respect to its real part. Evidently, this ratio is position dependent and the phenomenon is expected to be larger than the ratio $|x_1|/X_3^{\mathrm{r,t}}$ is, that is, closer to the boundary or, which is equivalent, at large horizontal offsets.

Equation (28) finally leads to the time-domain expressions for the electric-field constituents

$$E_2^{\mathrm{i,r,t}}(x_1, x_3, t) = \mu\, \partial_t \left[I(t) \overset{(t)}{*} G^{\mathrm{i,r,t}}(x_1, x_3, t)\right] \quad (42)$$

where $\overset{(t)}{*}$ denotes the time convolution. Further investigation into the effect of the different parameters on waveshapes requires a study via the numerical evaluation of the relevant integrals in (40)–(42). This is discussed in the next section.

VI. Feeding Electric Current Pulse Shapes

Two types of feeding electric current pulse shapes will be used: the power exponential pulse and the power exponential monocycle pulse [14], [15]. Their definitions and properties are given as follows.

A. Power Exponential Pulse

The power exponential pulse belongs to the class of *unipolar pulses*. Unipolar pulses do not change sign with time and have a single maximum in their absolute value. Unipolar pulses are typically suited for modeling electric currents that are associated with the discharge of an initially charged capacitor in an otherwise resistive electric circuit.

A convenient three-parameter unipolar pulse is the *power exponential pulse*, characterized by its *pulse amplitude* $I_{\max}$, its *pulse rise time* t_{r}, and the *power* ν of its initial increase with time

$$I(t) = I_{\max}\left(\frac{t}{t_{\mathrm{r}}}\right)^{\nu} \exp\left[-\nu\left(\frac{t}{t_{\mathrm{r}}} - 1\right)\right] H(t) \quad \text{with } \nu \geq 0 \quad (43)$$

where $H(t)$ denotes the *Heaviside unit step function*:

$$H(t) = \{0, 1/2, 1\} \text{ for } \{t < 0, t = 0, t > 0\}. \quad (44)$$

An example of a power exponential pulse is shown in Fig. 4.

B. Monocycle Pulse

In all cases where there is an electric or electronic circuit, no net electric charge is transported (as is the case in all closed electrically conducting loops), the condition

$$\int_{t=0}^{\infty} I(t)\mathrm{d}t = 0 \tag{45}$$

applies. The simplest manner to satisfy (45) is to take $I(t)$ to be a function with a single zero, a so-called *monocycle pulse*. The condition is elegantly accommodated by taking the pulse shape of a monocycle pulse to be the time differentiated one of a unipolar pulse. Then, the pulse rise time of the differentiated pulse manifests itself as the *zero crossing* of the constructed monocycle pulse. For the power exponential pulse (43), this results in

$$\begin{aligned} I(t) &= I_{\max}\,\partial_t\left[\left(\frac{t}{t_{\mathrm{r}}}\right)^{\nu}\exp\left[-\nu\left(\frac{t}{t_{\mathrm{r}}}-1\right)\right]\right]H(t)\\ &= I_{\max}\frac{\nu}{t_{\mathrm{r}}}\left(1-\frac{t}{t_{\mathrm{r}}}\right)\left(\frac{t}{t_{\mathrm{r}}}\right)^{\nu-1}\\ &\quad\times\exp\left[-\nu\left(\frac{t}{t_{\mathrm{r}}}-1\right)\right]H(t)\\ &\qquad\qquad\text{with } \nu\geq 1. \end{aligned} \tag{46}$$

In digital signal transfer, the first peak in each of the constituents in a monocycle pulse train is indicative of the binary value it represents. For these kinds of applications, it is customary to consider the corresponding peak value as the amplitude of the pulse. Furthermore, the zero crossing time $t_{0\mathrm{x}}$ is taken as one of its characteristics. The two extrema of the right-hand side of (46) follow from equating to zero its time derivative. This yields

$$\nu(\nu-1) - 2\,\nu^2 t/t_{0\mathrm{x}} + \nu^2(t/t_{0\mathrm{x}})^2 = 0 \tag{47}$$

which has the solutions

$$t/t_{0\mathrm{x}} = 1 \mp \nu^{-1/2}. \tag{48}$$

From this, it follows that:

$$t_{\mathrm{peak}} = (1-\nu^{-1/2})t_{0\mathrm{x}}. \tag{49}$$

Introducing the peak amplitude

$$I_{\mathrm{peak}} = I(t_{\mathrm{peak}}), \tag{50}$$

the *standard form* of (46) is obtained as

$$\begin{aligned} I(t) &= I_{\mathrm{peak}}\,N(\nu)\left(1-\frac{t}{t_{0\mathrm{x}}}\right)\left(\frac{t}{t_{0\mathrm{x}}}\right)^{\nu-1}\\ &\quad\times\exp\left[-\nu\left(\frac{t}{t_{0\mathrm{x}}}-1\right)\right]H(t)\\ &\qquad\qquad\text{with } \nu\geq 1 \end{aligned} \tag{51}$$

where

$$N(\nu) = \nu^{1/2}\left(\frac{1}{1-\nu^{-1/2}}\right)^{\nu-1}\exp(-\nu^{1/2}). \tag{52}$$

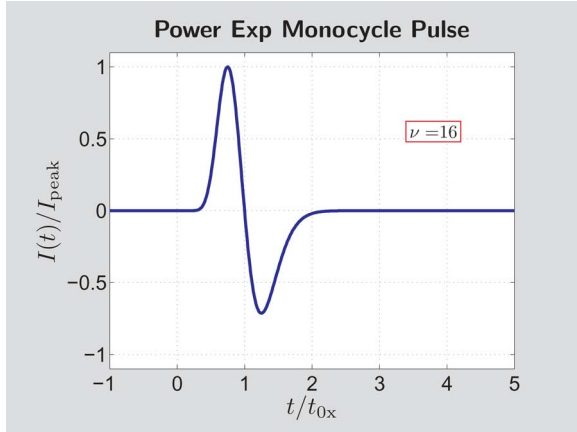

Fig. 5. Example of a monocycle pulse.

An example of a monocycle power exponential pulse is shown in Fig. 5.

VII. Illustrative Numerical Results

In this section, we present some illustrative numerical results for the aforementioned two types of pulse shapes of the feeding electric current: the unipolar pulse of the power exponential type and the monocycle pulse related to the first derivative of the power exponential pulse. The governing electromagnetic parameters in the configuration are: the *layer conductance ratio*

$$\eta_{\mathrm{L}} = \frac{G_{\mathrm{L}}}{Y} = G_{\mathrm{L}}Z \tag{53}$$

where $Y = (\epsilon/\mu)^{1/2}$ and $Z = (\mu/\epsilon)^{1/2}$, and the *layer admittance time constant*

$$\tau_{\mathrm{L}} = \frac{C_{\mathrm{L}}}{G_{\mathrm{L}}}. \tag{54}$$

Time snaps at certain locations and 2-D color density plots of the field distribution in space at successive time instants are computed.[1]

The generic time convolution integral in the representation of the different wave constituents is of the form

$$E(t) = \left[\int_{\tau=T}^{t} I(t-\tau)\frac{A(\tau)}{(\tau^2-T^2)^{1/2}}\,\mathrm{d}\tau\right]H(t-T). \tag{55}$$

To account for the inverse square-root singularity in the integrand at $\tau = T$, the following change of variable of integration is carried out:

$$\tau = T + (t-T)u^2 \text{ for } 0 < u < 1. \tag{56}$$

This transforms (55) into

$$\begin{aligned} E(t) = \Bigg[2\,(t-T)^{1/2}\int_{u=0}^{1} &I[(t-T)(1-u^2)]\\ &\times\frac{A[T+(t-T)u^2]}{[2\,T+(t-T)u^2]^{1/2}}\,\mathrm{d}u\Bigg]H(t-T). \end{aligned} \tag{57}$$

[1]A copy of the Matlab programs is available upon request from jianglj@hku.hk.

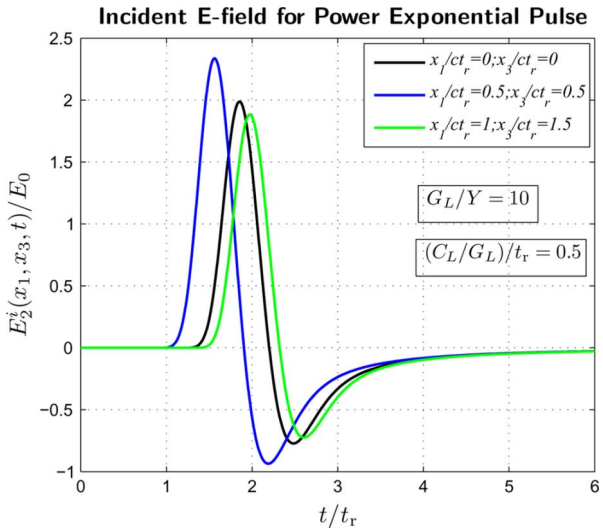

Fig. 6. Incident E-field when the feeding electric current pulse is a power exponential pulse.

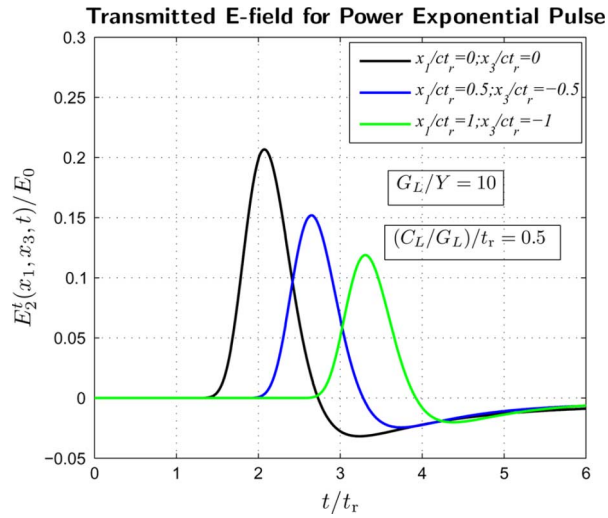

Fig. 8. Transmitted E-field when the feeding electric current pulse is a power exponential pulse.

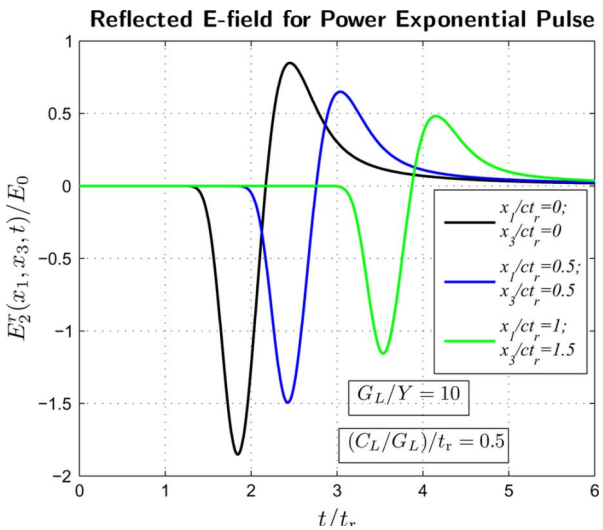

Fig. 7. Reflected E-field when the feeding electric current pulse is a power exponential pulse.

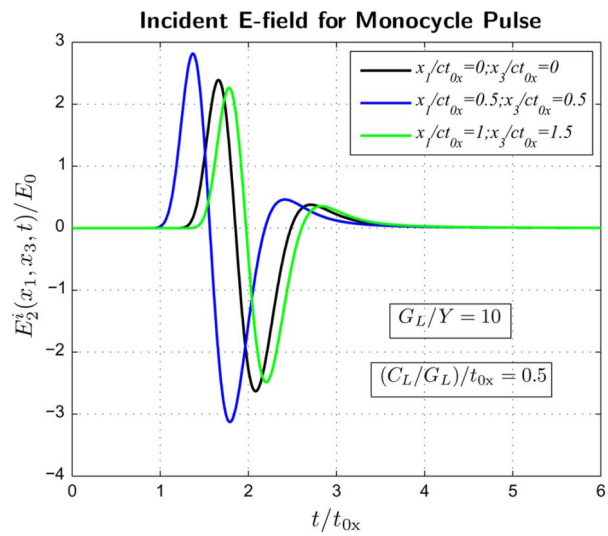

Fig. 9. Incident E-field when the feeding electric current pulse is a monocycle pulse.

Actually, $E_2^{\mathrm{i}}(x_1,x_3,t)$ admits a closed-form expression, whereas for $E_2^{\mathrm{r}}(x_1,x_3,t)$ and $E_2^{\mathrm{t}}(x_1,x_3,t)$, we use this method when calculating $G^{\mathrm{r}}(x_1,X_3^{\mathrm{r}},t)$ and $G^{\mathrm{t}}(x_1,X_3^{\mathrm{t}},t)$.

The numerical results of $E_2^{\mathrm{i}}(x_1,x_3,t), E_2^{\mathrm{r}}(x_1,x_3,t)$ and $E_2^{\mathrm{t}}(x_1,x_3,t)$ are computed using the proposed method and plotted. The first scenario computed uses the parameters $G_L/Y = 10, \tau_{\mathrm{L}}/t_{\mathrm{r}} = 0.5$ and $\tau_{\mathrm{L}}/t_{0\mathrm{x}} = 0.5$. E_0 is a constant. Figs. 6–8 are the resulting E-field time snaps at three specified locations corresponding to the power exponential pulse. The line source is located at $(0,0,1)ct_{\mathrm{r}}$. Fig. 6 shows the incident pulsed field at $(0,0,0^+)ct_{\mathrm{r}}$, $(0.5,0,0.5)ct_{\mathrm{r}}$ and $(1,0,1.5)ct_{\mathrm{r}}$. The dimensionless values of x_1/x_3^{i} equal 1, 1, and 2/3. Fig. 7 shows the reflected field at these three positions $(x_1/x_3^{\mathrm{r}} = 1,1,2/3)$. The power exponential pulse is obviously delayed and inverted in phase through the reflection on the thin highly conductive layer. Oscillations brought by $G^{\mathrm{r}}(x_1,X_3^{\mathrm{r}},t)$ are overwhelmed by the attenuation. This case also occurs in other figures related to reflected E-field and transmitted E-field (Figs. 8, 10–12 and 15–16). Fig. 8 shows the transmitted waves versus the time at three positions of the other side of the object layer: $(0,0,0^-)ct_{\mathrm{r}}, (0.5,0,-0.5)ct_{\mathrm{r}}$, and $(1,0,-1)ct_{\mathrm{r}}$. The dimensionless values of x_1/x_3^{t} are equal $-1,-1$ and -1. Only a small portion of the field passes through the thin layer due to the high contrast and conductivity. Figs. 9–11 are the E-field time snaps corresponding to the monocycle pulse for the same thin layer. The position of the line source is $(0,0,1)ct_{0\mathrm{x}}$. Fig. 12 is used to verify the boundary condition. We first draw the incident field, reflected field, and transmitted field at location $(0,0,0)ct_{0\mathrm{x}}$. We expect the continuity condition of the E-field to hold at $x_3 = 0$. Hence, the subtraction of the total E-field from both sides shall be zero, which means a flat line at 0. Fig. 12 demonstrates the validity of this property. Hence, it can be seen that the proposed method can reasonably predict the reflected wave and transmitted wave.

We also plot the figures of the field distribution in space at successive time instants for reflected wave and transmitted wave

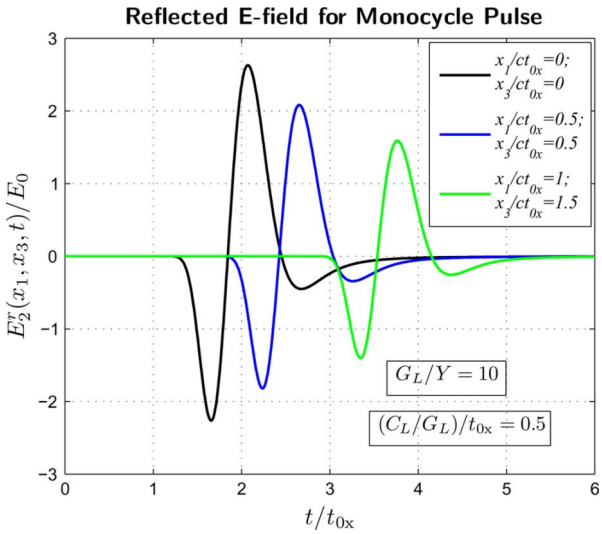

Fig. 10. Reflected E-field when the feeding electric current pulse is a monocycle pulse.

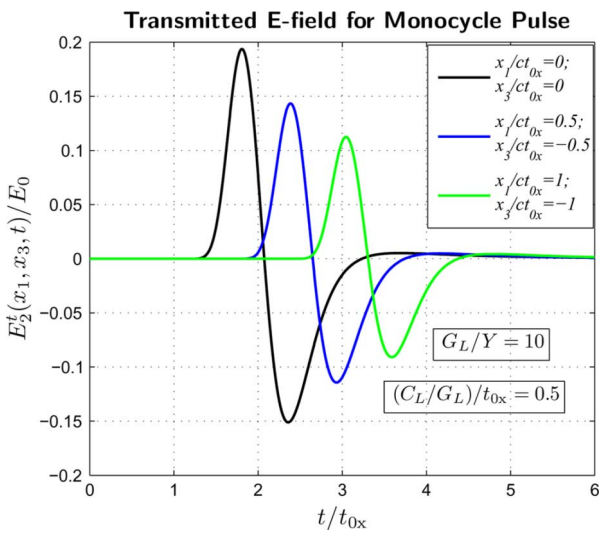

Fig. 11. Transmitted E-field when the feeding electric current pulse is a monocycle pulse.

(Figs. 13 and 14). The feeding electric current pulse is the monocycle pulse.

In the second case, we consider a 30-μm-thick copper layer using the same method to obtain the incident wave, reflected wave, and transmitted wave. This type of copper layer is frequently used for printed-circuit boards (PCBs). The feeding electric current pulse is the monocycle pulse. The reflected and transmitted figures are given in Figs. 15 and 16 since the incident figure is the same as the aforementioned one. Comparing Figs. 15 and 16 with Figs. 10 and 11, we can see that the transmitted wave is much smaller because the high contrast layer is much thicker in this second case. To verify this method, we now calculate the generalized transmission coefficient of a three-layer medium. The thin sheet is located in the middle. The generalized transmission coefficient at the lower surface of the sheet in the frequency domain is

$$\tilde{T}_{1,3} = \frac{T_{1,2}}{1 - R_{2,1}R_{2,3}e^{2ik_2d_0}}\, T_{2,3}\, e^{ik_2d_0}. \tag{58}$$

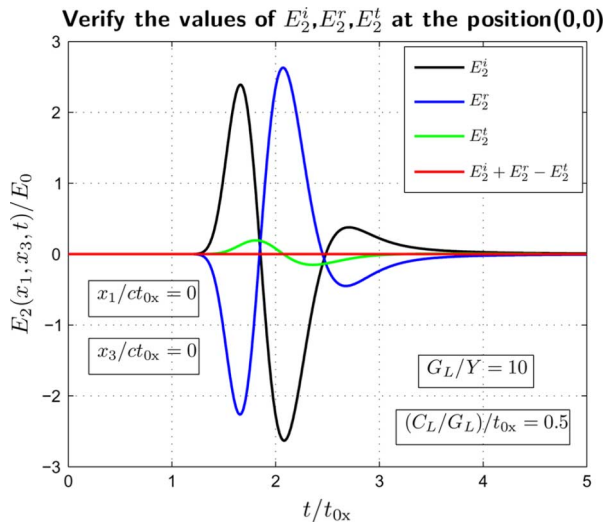

Fig. 12. Verifying the boundary condition when the feeding electric current pulse is a monocycle pulse.

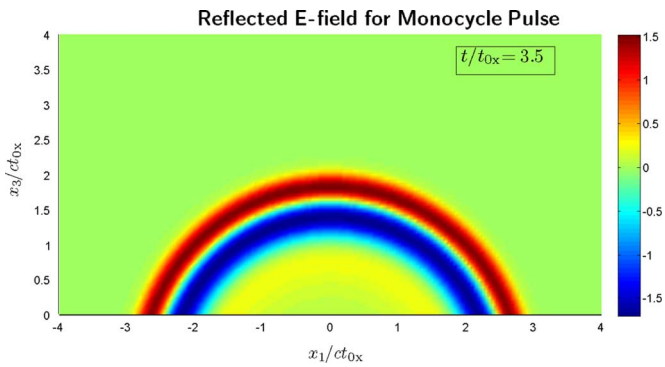

Fig. 13. Reflected E-field density plot when the feeding electric current pulse is a monocycle pulse.

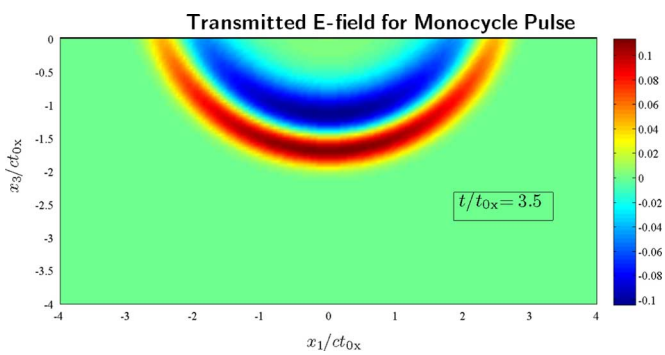

Fig. 14. Transmitted E-field density plot when the feeding electric current pulse is a monocycle pulse.

Here, $T_{1,2}$ and $T_{2,3}$ are transmission coefficients at the interfaces from medium 1 (air) to medium 2 (thin sheet) and from medium 2 to medium 3 (air), respectively. k_2 is the wave number in medium 2. Fig. 17 shows the magnitude of $\tilde{T}_{1,3}$ corresponding to the first scenario, that is, $G_L/Y = 10$ and $\tau_L/t_{0x} = 0.5$. The observation point in the frequency domain is 100 MHz ($t_{0x} = 1 * 10^{-8}$s). Fig. 18 gives the result of $\tilde{T}_{1,3}$ when the middle layer is copper. In both figures, we can find that the transmitted wave of the incident wave matches well with our results

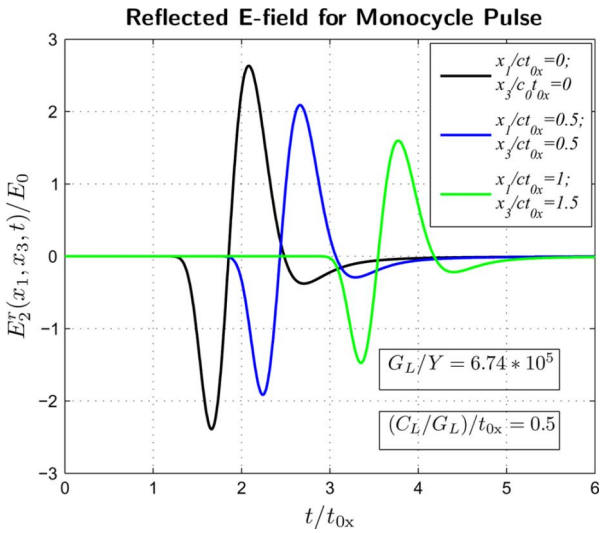

Fig. 15. Reflected E-field for the copper sheet when the feeding electric current pulse is a monocycle pulse.

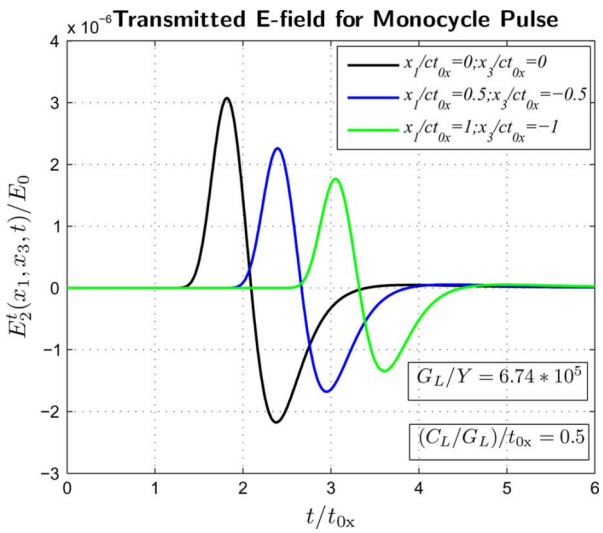

Fig. 16. Transmitted E-field for the copper sheet when the feeding electric current pulse is a monocycle pulse.

using the proposed method if we compare the value of the transmission coefficient at the observation point with the ratio of the maximum of the transmitted wave over the maximum of the incident wave. In addition, we use a popular commercial tool for cross checking, in which the plane wave is employed as the port excitation. Fig. 19 is the simulation result using the commercial tool for the first case. From the figure, we can find that the ratio is close to the generalized transmission coefficient and our numerical result. This means that our setup for the model in the commercial tool is correct. An explicit merit of our method is high efficiency since it almost took 36 h to obtain the transient results if the commercial tool is used. We also use this tool to simulate the copper case. Unfortunately, it fails. The time-consuming drawback and the failure for a high-contrast thin layer of the commercial tool, on the other hand, set off the value of our method.

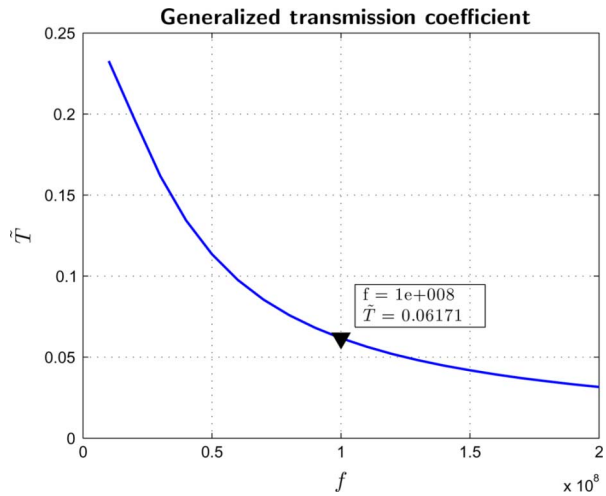

Fig. 17. Generalized transmission coefficient for the monocycle pulse, when parameters are set as $G_L/Y = 10$ and $\tau_L/t_{0x} = 0.5$.

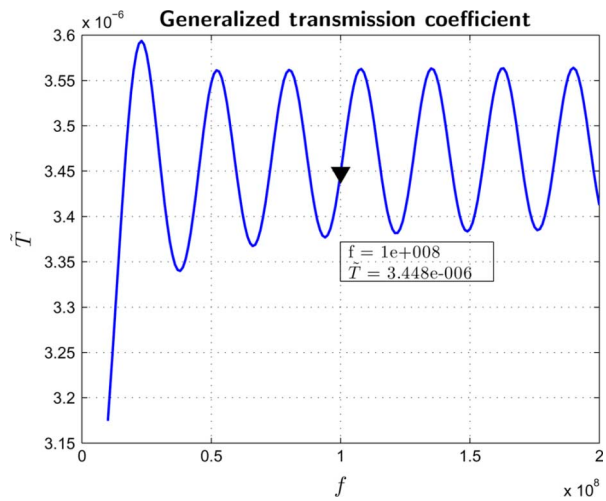

Fig. 18. Generalized transmission coefficient for the monocycle pulse, when parameters are set as $G_L/Y = 6.74 * 10^5$ and $\tau_L/t_{0x} = 0.5$ (i.e., the copper case).

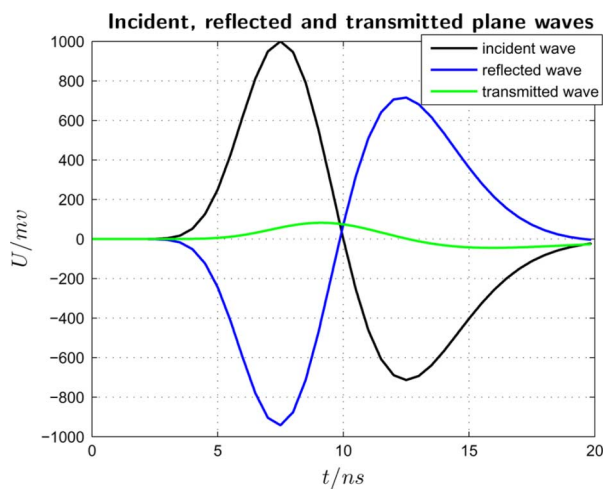

Fig. 19. Simulation results from the commercial tool for the monocycle pulse, when parameters are set as $G_L/Y = 10$ and $\tau_L/t_{0x} = 0.5$.

VIII. Conclusion

Via an extension of the Cagniard–de Hoop method for analyzing the pulsed-field behavior in layered configurations, closed-form analytic time-domain expressions have been derived for the EM-field constituents that are generated by a pulsed line source of electric current in the presence of a thin, highly contrasting layer with dielectric and conductive properties in a 2-D model setting. It provides a novel solution for the field computation of line sources on top of the thin conductive layers frequently encountered in integrated-circuit and printed-circuit-board designs. Numerical results based on the field expressions obtained can serve as an indication as to the possibilities of applying the pertaining thin-sheet (approximate) boundary conditions in codes for computational electromagnetics.

Acknowledgment

The authors would like to thank the anonymous reviews for suggestions to improve this manuscript and to add more material.

References

[1] A. T. De Hoop and L. Jiang, "Pulsed EM field response of a thin, high-contrast, finely layered structure with dielectric and conductive properties," *IEEE Trans. Antennas Propag.*, vol. 57, no. 8, pp. 2260–2269, Aug. 2009.

[2] A. T. De Hoop and L. J. Jiang, "Reflection and transmission of line-source excited pulsed EM fields at a thin, high-contrast layer with dielectric and conductive properties," in *Proc. IEEE Int. Symp. Antennas Propag.*, 2011, pp. 2404–2406.

[3] L. Cagniard, *Réflexion et Réfraction des Ondes Séismiques Progrressives*. Paris, France: Gauthier-Villars, 1939.

[4] L. Cagniard, *Reflection and Refraction of Progressive Seismic Waves*. New York: McGraw-Hill, 1962.

[5] A. T. De Hoop, "A modification of Cagniard's method for solving seismic pulse problems," *Appl. Scientif. Res.*, vol. B8, pp. 349–356, 1960.

[6] A. T. De Hoop, "Pulsed electromagnetic radiation from a line source in a two-media configuration," *Radio Sci.*, vol. 14, no. 2, pp. 253–268, Mar./Apr. 1979.

[7] K. J. Langenberg, "The transient response of a dielectric layer," *Appl. Phys.*, vol. 3, pp. 179–188, 1974.

[8] D. V. Widder, *The Laplace Transform*. Princeton, NJ, USA: Princeton Univ. Press, 1946.

[9] A. T. De Hoop, *Handbook of Radiation and Scattering of Waves*. London, U.K.: Academic Press, 1995. [Online]. Available: www.atdehoop.com

[10] J. P. Schouten, "A new theorem in operational calculus together with an application of it," *Physica*, vol. 1, pp. 75–80, 1934.

[11] J. P. Schouten, *Operatorenrechnung*. Berlin, Germany: Springer-Verlag, 1961.

[12] B. Van Der Pol, "A theorem on electrical networks with an application to filters," *Physica*, vol. 1, pp. 521–530, 1934.

[13] B. Van Der Pol and H. Bremmer, *Operational Calculus Based on the Two-Sided Laplace Transform*. Cambridge, U.K.: Cambridge Univ. Press, 1950.

[14] A. T. de Hoop and I. E. Lager, "Pulsed fields EM interference analysis in digital signal wireless Interconnects," in *Proc. 41st Eur. Microw. Conf.*, Manchester, U.K., Oct. 2011, pp. 313–316.

[15] I. E. Lager and A. T. de Hoop, "Loop-to-loop pulsed electromagnetic field wireless signal transfer," presented at the 6th Eur. Conf. Antennas Propag., Prague, Czech Republic, Mar. 2012.

Adrianus T. de Hoop (M'00) was born on December 24, 1927, in Rotterdam, The Netherlands. He received the M.Sc. degree in electrical engineering (Hons.) and the Ph.D. degree in the technological sciences (Hons.) from Delft University of Technology, Delft, The Netherlands, in 1950 and 1958, respectively.

He served Delft University of Technology as an Assistant Professor (1950–1957), Associate Professor (1957–1960), and Full Professor in Electromagnetic Theory and Applied Mathematics (1960–1996). Since 1996, he has been Lorentz Chair Emeritus Professor in the Faculty of Electrical Engineering, Mathematics and Computer Science, Delft University of Technology. In 1970, he founded the Laboratory of Electromagnetic Research, Delft University of Technology, which has developed into a world-class center for electromagnetics. His interdisciplinary insights and methods in this field can be found in his *Handbook of Radiation and Scattering of Waves* (London, 1995), with wave-field reciprocity serving as one of the unifying principles governing direct and inverse scattering problems and wave propagation in complex (anisotropic and dispersive) media. He spent a year (1956–1957) as a Research Assistant with the Institute of Geophysics, University of California at Los Angeles, Los Angeles, CA, USA, where he pioneered a modification of the Cagniard technique for calculating impulsive wave propagation in layered media, later to be known as the "Cagniard-DeHoop technique." Since 1982, he has, on a regular basis, been a Visiting Scientist with Schlumberger-Doll Research, Ridgefield, CT, USA, where he contributes to research on geophysical applications of acoustic, electromagnetics, and elastodynamic waves. Grants from the "Stichting Fund for Science, Technology and Research" (founded by Schlumberger Ltd.) supported his research at Delft University of Technology. Recently, he is exploring a method for computing pulsed electromagnetic fields in strongly heterogeneous media with application to (microscale or nanoscale) integrated circuits. His research interests are in the broad area of wave-field modeling in acoustics, electromagnetics, and elastodynamics.

Dr. de Hoop is a Member of the Royal Netherlands Academy of Arts and Sciences and a Foreign Member of the Royal Flemish Academy of Belgium for Science and Arts. He holds an Honorary Doctorate in the Applied Sciences from Ghent University, Belgium (1981). He was awarded the 1989 Research Medal of the Royal Institute of Engineers in the Netherlands, the IEEE 2001 Heinrich Hertz Gold Research Medal, and the 2002 URSI (International Scientific Radio Union) Balthasar van der Pol Gold Research Medal. In 2003, H.M. the Queen of The Netherlands decorated him "Knight in the Order of the Netherlands Lion."

Ling Ling Meng (S'13) received the B.S. degree in information science and engineering from Chien-Shiung Wu College (Honor Class), Southeast University, Nanjing, China, in 2011 and is currently pursuing the M.Phil. degree in electrical and electronic engineering at the University of Hong Kong. Hong Kong, China.

Her main work is to obtain the numerical results in this paper.

Li Jun Jiang (SM'13) received the B.S. degree in electrical engineering from the Beijing University of Aeronautics and Astronautics, Beijing, China, in 1993, the M.S. degree in electronic engineering from Tsinghua University, Beijing, China, in 1996, and the Ph.D. degree in computational electromagnetics from the University of Illinois at Urbana-Champaign, Champaign, IL, USA, in 2004.

From 1996 to 1999, he was an Application Engineer with the Hewlett-Packard Company, Beijing, China. Since 2004, he has been the Postdoctoral Researcher, the Research Staff Member, and the Senior Engineer at IBM T.J. Watson Research Center, Yorktown Heights, NY, USA. Since 2009, he has been an Associate Professor with the Department of Electrical and Electronic Engineering, University of Hong Kong, Hong Kong, China. He has served as the reviewer of many primary professional journals, special sessions organizer for many international conferences, and chair of many international conference sessions. His research interests focus on electromagnetics, electromagnetic compatibility/electromagnetic interference, antennas, multidisciplinary electronic design automation solutions, RF and microwave technologies, and high-performance computing.

Dr. Jiang received the HP STAR Award in 1998. In 2003, he received the IEEE MTT Graduate Fellowship Award, and in 2004, the Y.T. Lo Outstanding Research Award. In 2008, he received the IBM Research Technical Achievement Award and he was the Semiconductor Research Cooperation (SRC) Industrial Liaison for several academic projects. Since 2009, he has been the SRC Packaging High Frequency Topic TT Chair. He has served as Technical Committee Member for IEEE EDAPS since 2010, the Scientific Committee Member of 2010 IEEE SMEE, and the Associate Guest Editor of Proceedings of the IEEE since 2011. He was the Scientific Consultant of HK ASTRI in 2010. He is a member of the IEEE Antennas and Propagation Society, IEEE Microwave Theory and Techniques Society, Applied Computational Electromagnetics Society, and Sigma Xi.